Chemical Science

EDGE ARTICLE

View Article Online
View Journal

Mechanism and active site of photocatalytic water splitting on titania in aqueous surroundings

Cite this: DOI: 10.1039/c3sc53385a

Wei-Na Zhao and Zhi-Pan Liu*

Photocatalytic water splitting is regarded as an important route for generating renewable energy. Here, charged-slab first principles calculations integrated with a periodic continuum solvation model is utilized to analyze the initiating steps of water splitting on the two most common TiO_2 surfaces, namely, rutile (110) and anatase (101), at the solid–water interface. It is found that the first proton removal of water (H_2O + hole$^+$ → OH + H^+) is sensitive to the crystalline phase and surface. The rutile (110) surface is more active for water splitting, with the calculated barrier of O–H bond breaking being 0.2 eV lower compared to that on anatase (101). The higher activity of rutile is not due to the redox level of the hole (the position of the valence band maximum), but caused by the more favorable local bonding geometry of the surface. Unexpectedly, the photogenerated hole does not promote O–H bond breaking, and the charge transfer occurs after the H_2O dissociation when the surface O nearby the dissociated OH anion traps the hole. The solvation plays an important catalytic role to stabilize and remove protons from the reaction site, which effectively inhibits the charge-recombination of the dissociated OH anion with the proton. The theory presented here shows that the chemical properties of the surface play a significant role in the photocatalytic process, and a strategy based on simple structural parameters is proposed towards the design of new photocatalysts.

Received 10th December 2013
Accepted 12th February 2014

DOI: 10.1039/c3sc53385a

www.rsc.org/chemicalscience

Published on 13 February 2014. Downloaded by Fudan University on 27/03/2014 15:09:31.

1. Introduction

Recent years have seen enormous research interest in direct water splitting using solar light radiation.[1] Among various photoactive materials, titania-based composites are one of the most promising catalysts for water splitting, not least because of the high stability under (violet) radiation and the ability for water oxidation even on bare TiO_2. To date, one major concern for water splitting on titania polymorphs, the practically utilized photocatalysts, is to identify the active site.[2] Due to the lack of a fundamental understanding of the elementary steps of water splitting, how to design better photocatalyst for direct water splitting remains largely elusive. A theory to clarify the roles of the photo-generated holes, the catalyst surface and solvation in relation to the water oxidation kinetics is thus urgently required.

Since the discovery of photocatalytic water splitting on TiO_2,[3] much effort has been devoted to search for the active site of TiO_2. The water oxidation reaction can be written as H_2O + hole$^+$ → $1/2O_2$ + $2H^+$, which is an extremely difficult reaction under heat-driven conditions and occurs only above +1.23 V *vs.* SHE under electrochemical conditions. Matsumura *et al.*[4] showed that water can be photocatalytically oxidized into oxygen on rutile powder with a fairly high efficiency of 9% (iron(III) ions as the electron acceptor), and the quantum efficiency of oxygen evolution is evaluated to be 17% on rutile particles.[5] They attributed the high activity to the preferential adsorption of Fe^{III} ions on rutile. Although the rutile phase is believed to possess a higher photoactivity for oxidation,[6] recent studies from well-controlled nanoscience challenge this view, showing that the presence of anatase would enhance the activity or even dominate the oxidation reaction. For example, Ohno *et al.*[7] found a clear synergistic effect of P25 TiO_2 powder (the proportion of the crystalline phases anatase and rutile is about 4 : 1 (ref. 8)) for the photocatalytic oxidation of naphthalene. Similarly, Zhang *et al.*[9] found that the presence of a phase junction between anatase and rutile can greatly enhance the photocatalytic activity of TiO_2 by up to four times, as evidenced by Raman spectroscopy and high-resolution TEM. On the other hand, Kavan *et al.*[10] synthesized single crystals of TiO_2 anatase containing 0.22% of Al and traces of V, Zr, Nb and La, and found that the photoelectrochemical oxidation of water could occur efficiently on both rutile and anatase (with the incident photons at ~300 nm), but the reduction of water to H_2 (by photogenerated electrons) only proceeded spontaneously on anatase. Higher photo-oxidation ability of anatase (101) surfaces compared to rutile has also been reported from methanol photo-oxidation on well-defined single-crystal surfaces.[11]

Theoretical studies would be highly desirable to resolve the kinetic data of water oxidation on various catalyst surfaces.

Shanghai Key Laboratory of Molecular Catalysis and Innovative Materials, Department of Chemistry, Key Laboratory of Computational Physical Science (Ministry of Education), Fudan University, Shanghai 200433, China. E-mail: zpliu@fudan.edu.cn

Published on 13 February 2014. Downloaded by Fudan University on 27/03/2014 15:09:31.

However, such investigations on the solid–liquid interface photocatalysis are rather limited,[12] despite the fact that first principles calculations have been much utilized for predicting the thermodynamic[13] and kinetic properties[14] of heterogeneous catalysis in the last twenty years. Obviously, this is due to intrinsic complexity arising from the electrical double-layer at the solid–liquid interface and the photo irradiation conditions. There are two critical issues that are important to photocatalysis but not well treated in the conventional density functional theory (DFT) packages, namely, (i) the modelling of the solid–liquid interface, essential for modelling the strong polarization of the charged surfaces in solution; (ii) the inaccuracy of current DFT functionals in describing the redox levels of oxides (*e.g.* the band gap and the valence band position relative to the H_2O/H_2 and H_2O/O_2 levels).[15] These have led to great challenges to compute the photocatalytic reaction kinetics as driven by the excess holes/electrons accumulated on the catalyst surfaces.

Here we report the first theoretical analysis on the mechanism and the possible active site for water oxidation on titania. Large-scale calculations based on DFT integrated with a periodic continuum solvation model (DFT/CM-MPB method) are utilized for modeling the charge-driven photo-oxidation process at the solid–liquid interface involving two common surfaces of two typical TiO_2 phases, *i.e.* anatase (101) and rutile (110). We demonstrate that the charged-slab DFT/CM-MPB method allows us to evaluate in detail the water oxidation kinetics and compare the activity across the surfaces within a unified theoretical framework, in which the electrical double-layer effect due to the surface charging and the redox level of the oxide surfaces can be properly treated simultaneously.

2. Methodology and calculation detail

2.1 DFT/CM-MPB methods and surface models

All DFT calculations were performed using SIESTA,[16] where optimized double-ζ plus polarization numerical atomic orbital basis sets[17] were utilized along with the Troullier–Martins norm-conserving pseudopotentials.[18] The exchange correlation functional utilized is at the generalized gradient approximation level proposed by Perdew, Burke and Ernzerhof (GGA-PBE).[19] The semi-core 3s and 3p states of Ti were included in all calculations. The cutoff for the real space grid was set as 250 Ry. The L-BFGS method was employed for geometry relaxation until the maximal forces on each relaxed atom were less than 0.1 eV $Å^{-1}$. The finite difference method is utilized to compute the eigenvalues of Hessian and to correct the zero point energy (ZPE) of the system. All transition states (TSs) of the reaction were searched using Constrained Broyden Minimization and Constrained Broyden Dimer methods designed for treating complex reaction systems.[20]

The solid–liquid interface is modeled using a recently-developed periodic CM-MPB method,[21] which can account for the long-range electrostatic interaction due to solvation between the surface and solution. Using this approach, the surface can be charged to mimic the charged surface under photocatalytic conditions, and the counter charge is distributed as point charges outside the surface (the vacuum region) in the manner determined by the MPB equation. Such a distribution mimics the realistic electrolyte distribution and is thus more physically meaningful compared to the homogeneous background charge in standard periodic DFT calculations.[22] We have recently utilized this approach for modeling electrochemical reactions on metal surfaces,[23] and a detailed description on the methodology can be found in our recent work.[24] The dielectric constant of the bulk water solution is set as 78.36 according to the experimental value. Within the CM-MPB framework, it is convenient to align the band position of the extended surfaces with the same solution level (*e.g.*, ~15 Å away from the surface).

The rutile (110) and anatase (101) surfaces (Fig. 1) are both modeled by a rectangular unit cell of six TiO_2 layer slabs with the lattice parameters of (14.834 × 13.145 Å, 360 atoms) and (10.398 × 15.264 Å, 288 atoms), respectively, and the vacuum spacing is generally larger than 30 Å. The DFT optimized lattice parameters are ($a = b = 3.81$, $c = 9.67$ Å) for anatase and ($a = b = 4.65$, $c = 2.97$ Å) for rutile crystal, which agrees well with the experimental lattice (anatase: $a = b = 3.78$, $c = 9.49$ Å; rutile: $a = b = 4.59$, $c = 2.96$ Å). In all calculations, the central two TiO_2 layers are fixed at bulk-truncated positions while the other layers are allowed to relax. Due to the large unit cell, only the Γ-point was utilized. The convergence of the k-point mesh and basis set in calculating the barrier has been checked for key reactions in our recent work.[25]

It should be mentioned that the hydroxyl groups are present under experimental conditions (aqueous solution).[1g] However, the modelling of the likely composition of adsorbed hydroxyl groups together with water molecules requires detailed knowledge on the free energy equilibrium of the species on the surface in contact with the aqueous environment, which is highly challenging for theoretical simulations. On the other hand, since the chemical reactions are local, here we utilize the explicit solvation by adding a few water molecules nearby the reactants, together with the implicit CM-MPB model which takes into account the long-range solvent polarization to simulate the reactions at the solid–liquid interface. The same hybrid approach has been utilized in the group for understanding a range of electrocatalytic and photocatalytic reactions on surfaces.[24–26] We believe that the hybrid approach is able to provide insights into the photocatalytic water oxidation kinetics.

2.2 Charged-slab DFT/CM-MPB calculations for band level correction

For photoreaction on semiconducting catalysts, the conduction-band minimum (CBM) and valence-band maximum (VBM)

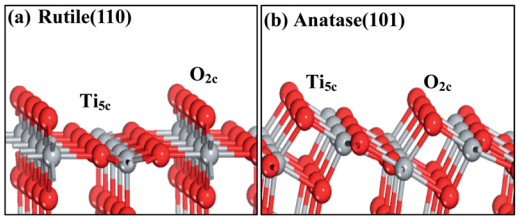

Fig. 1 (a) The rutile (110) and (b) anatase (101) surfaces. Ti, gray; O, red.

This journal is © The Royal Society of Chemistry 2014

Published on 13 February 2014. Downloaded by Fudan University on 27/03/2014 15:09:31.

levels of the system are critical, which measure the chemical potential of photo-generated holes/electrons and thus determine the thermodynamic tendency for a reaction to occur. Hence, the accurate computation of the CBM and VBM levels are the prerequisites for understanding the kinetics of photocatalytic reactions. However, due to the self-interaction problem[27] in density functionals, there is a tendency for the delocalization of electrons using the local density approximation (LDA) and its generalized gradient extension (GGA), which results in the underestimation of the band gap and the wrong VBM and CBM levels.

Among the attempts devoted to tackle the gap problem of DFT, the recently-developed Δ-sol method[22] is an attractive approach, which utilizes the total energy of the charged system to deduce the gap ($E_{gap} = E_{CBM} - E_{VBM}$), as written in eqn (1)–(3), without recourse to heavy-demanding high-level quantum mechanics calculations. Analogous to the Δ-SCF method for finite systems that shows improvements for the HOMO–LUMO gap prediction,[27,28] the Δ-sol method can reasonably avoid the delocalization error by confining the added charge to a volume that is commensurate with the range of the screening effects. The Δ-sol method involves fitted parameters on the system size that were optimized for a set of bulk materials, and it cannot be straightforwardly applied to the surface system.

$$E_{gap} = [E(N_0 + n) + E(N_0 - n) - 2E(N_0)]/n \quad (1)$$

$$E_{VBM} = [E(N_0 - n) - E(N_0)]/n \quad (2)$$

$$E_{CBM} = [E(N_0 + n) - E(N_0)]/n \quad (3)$$

We have extended the idea to surface systems where the photocatalytic reactions occur.[29] Here we briefly introduce the approach and utilize this method for the rutile and anatase surfaces. To extend the Δ-sol method to surface systems, two key issues inherent to the charged-cell calculations must be properly addressed: (1) the image–charge interaction error due to the neutralizing counter-charge required in periodic system calculations; (2) the optimum surface cell size for the added charge on the surface. In fact, the first problem can be largely avoided by using the DFT-CM/MPB approach, because the neutralizing counter charge is distributed outside the surface region, following the MPB equation, and the large dielectric constant of water can effectively screen the image–charge interaction. To search for the optimum unit cell size for the surface system, we can calculate the band structure of a bare oxide surface at different surface charge conditions. Fig. 2 shows that with the increase of the surface charge, the band gaps of the rutile and anatase surfaces increase, which is similar to those in finite systems.[22]

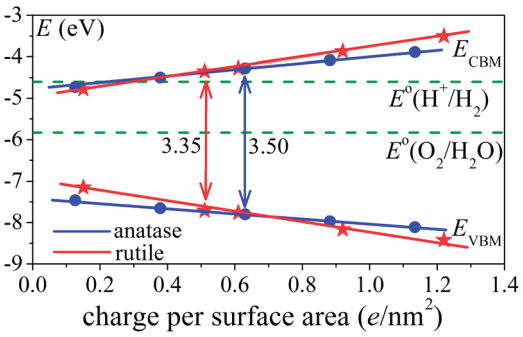

Fig. 2 The variation of the gap (E_{gap}), the level of VBM (E_{VBM}) and the level of CBM (E_{CBM}) with the added charge per surface area for anatase and rutile, as calculated from the charged-slab DFT/CM-MPB method. The standard equilibrium potential of H^+/H_2 and O_2/H_2O are also shown for the guide of eye (the absolute potential of SHE is taken as 4.6 V (ref. 30)).

As shown in Fig. 2, for both rutile and anatase, a window of the surface charge, *i.e.* 0.45–0.65 e nm^{-2}, can reproduce reasonably the experimental values (rutile: $E_{gap} \sim 3.0$ eV, $E_{VBM} \sim 3.0$ V *vs.* SHE and $E_{CBM} \sim 0$ V *vs.* SHE;[31] anatase: $E_{gap} \sim 3.2$ eV, $E_{VBM} \sim 3.0$ V *vs.* SHE and $E_{CBM} \sim -0.2$ V *vs.* SHE[1d]). For photocatalytic reactions, the local surface charge has to be one (either +1 or −1 of the hole/electron). In view of the 0.45–0.65 e nm^{-2} window, it is indicated that only a certain size of the unit cell is allowed in order to reproduce the experimental values. In this work, the large rectangle unit cells are selected for anatase (10.398 × 15.264 Å) with a surface charge density of 0.63 e nm^{-2} and rutile (14.834 × 13.145 Å) with a surface charge density of 0.51 e nm^{-2}. These slabs can be explicitly charged by +2 or −2 (two symmetrical surfaces per slab[24]), and the predicted E_{gap}, E_{VBM} and E_{CBM} for anatase are 3.50 eV, 3.20 V *vs.* SHE and −0.30 V *vs.* SHE, and those for rutile are 3.35 eV, 3.11 V *vs.* SHE and −0.25 V *vs.* SHE, respectively. These values are generally close to the experimental data. The charged-slab approach allows the quantitative evaluation of the charge-driven reaction kinetics with reasonable VBM and CBM levels.

To further verify the results from the charged DFT/CM-MPB calculations for reaction kinetics, we also utilized the hybrid functionals as implemented in the CP2K/QUICKSTEP[32] package for computing the barrier to the key reactions. In CP2K, the hybrid functionals, such as HSE06, are available for treating large oxide surface systems thanks to the auxiliary density matrix method[33] for computing the Hartree–Fock exchange. The calculated band gap using the above setups for rutile and anatase are 3.12 and 3.62 eV from the HSE06 functional, respectively, which are consistent with previous work[34] and are also compatible with those (3.35 and 3.50 eV) from the charged-slab DFT/CM-MPB calculations shown above. In this work, we found that the difference between charged-slab PBE and the HSE06 functional in the calculated barrier is generally small (*e.g.* the barriers of the O–H cleavage differ by ~0.1 eV using the two functionals; see Section 3.2).

2.3 Theoretical approach for calculating the kinetics of photocatalytic reactions

To investigate the photocatalytic kinetics on solid surfaces, the most practical approach is to focus on the electron/hole-driven redox chemistry, assuming that the intra-band de-excitation has taken place after the separation of the photo-generated exciton. This is reasonable as the temporal scale for electron relaxation is ~ps, being much shorter than that for charge recombination.[35]

Published on 13 February 2014. Downloaded by Fudan University on 27/03/2014 15:09:31.

With this assumption, the surface redox chemistry can be considered as the surface reaction occurring in the presence of an excess electron or hole at the solid–liquid interface. This reduces the computational task to model appropriately the charged (not "excited-state") systems. In this work, the DFT/CM-MPB method is used to calculate the charged surface systems.

Specifically, for a photocatalytic reaction, such as HA dissociation into A and H^+, we can always decompose the reaction into a number of elementary steps and then calculate the free energy change of the elementary steps. For example, for the charging of an adsorbed HA molecule on a surface (HA/sur) by a photo-generated hole, HA/sur + $h^+ \rightarrow [HA/sur]^+$, the free energy change ΔG can be calculated by

$$\Delta G_1 = G([HA/sur]^+) + G(sur) - G(sur^+) - G(HA/sur) \quad (4)$$

where the term $(G(sur^+) - G(sur))$ divided by the Faraday constant, *i.e.* $(G(sur^+) - G(sur))/F$, should be the absolute electrostatic potential of the hole (U_h) at the VBM of the surface, which can be obtained from the charged-slab DFT/CM-MPB calculations, as detailed above. In this work, U_h is determined to be 2.80 V for rutile (110) and 3.20 V for anatase (101) *vs.* SHE according to $G(sur) - G(sur^+)$, where the surface structural relaxation in the presence of holes is also considered. Obviously, a realistic estimation of VBM and thus U_h is a must for evaluating the activity of the photocatalytic oxidation (otherwise the computed reaction barrier will be incorrect due to the wrong chemical potential of the holes).

For the reactions involving H^+, *e.g.* $[H/sur]^+ \rightarrow sur + H^+(aq)$, the free energy change ΔG can be calculated by

$$\Delta G_2 = G(H_{aq}^+) + G(sur) - G([A + H/sur]^+) = 1/2G(H_2) + 4.6\ eV + G(sur) - G([A + H/sur]^+) \quad (5)$$

where the free energy change in the SHE reference electrode is utilized:

$$\Delta G_{SHE} = 1/2G(H_2) - G(H_{aq}^+) + 4.6\ eV = 0. \quad (6)$$

3. Results

For water oxidation, the first proton removal ($H_2O^* + hole^+ \rightarrow OH^* + H^+(aq)$; hereafter the superscript * indicates the adsorbed state) is known to be the key kinetic step (see our previous work[36] where the overall mechanism of water oxidation is computed from thermodynamics and compared with experimental observations[2b]), which involves both O–H bond breaking and the hole transfer. In this work, we will quantify the kinetics of this step on two TiO_2 surfaces and compare the activity difference between the two surfaces. There are three likely routes for the first proton removal, which differs in the sequence of the O–H bond breaking and the charge transfer, as outlined below.

(i) Hole-promoted water dissociation: the charge (hole) transfers from bulk to adsorbed water, leading to its subsequent dissociation, *i.e.* $H_2O^* + hole^+ \rightarrow H_2O^{+*} \rightarrow OH^* + H^{+*}$; in this route, the hole promotes the water dissociation.

(ii) Homolytic water splitting: water dissociates homolytically, followed by charge transfer from bulk to the adsorbed H, *i.e.* $H_2O^* \rightarrow OH^* + H^*$; $H^* + hole^+ \rightarrow H^{+*}$.

(iii) Heterolytic water splitting: water dissociates heterolytically, followed by charge transfer from bulk to adsorbed OH, *i.e.* $H_2O^* \rightarrow OH^{-*} + H^{+*}$; $OH^{-*} + hole^+ \rightarrow OH^*$.

3.1 The adsorbed species and their relative band position

To provide insights into the mechanism and the kinetics, we have first calculated the geometrical and electronic structure of the initial state (IS) and the possible final states (FS) of the first proton removal reaction, namely, the adsorbed H_2O and the coadsorbed OH and H (dissociated H_2O) at the solid–liquid interface. Due to the three possible reaction routes as mentioned above, the surfaces considered for the IS and FSs are either neutral or positively-charged (with hole). The optimized structures of the adsorbed H_2O (state 1) and the dissociated H_2O (state 2) in aqueous solution (with both explicit and implicit H_2O solvation) are shown in Fig. 3.

For H_2O adsorption, water adsorbs perpendicularly on a surface five-coordinated Ti (Ti_{5c}) site *via* its O end forming a O–Ti_{5c} bond, consistent with the previous calculations.[37,38] The other water molecules near to the adsorbed H_2O interact with the adsorbed H_2O and the lattice O through hydrogen bonding, which are ~2.50 Å above the surface forming the weakly-bound water layer. Compared to on the neutral surface, the O–Ti_{5c} distance is shortened slightly on the positively-charged surface, indicating increased O–Ti bonding due to the electrostatic interaction. Next, we calculated the adsorption free energy of the H_2O on the surface,

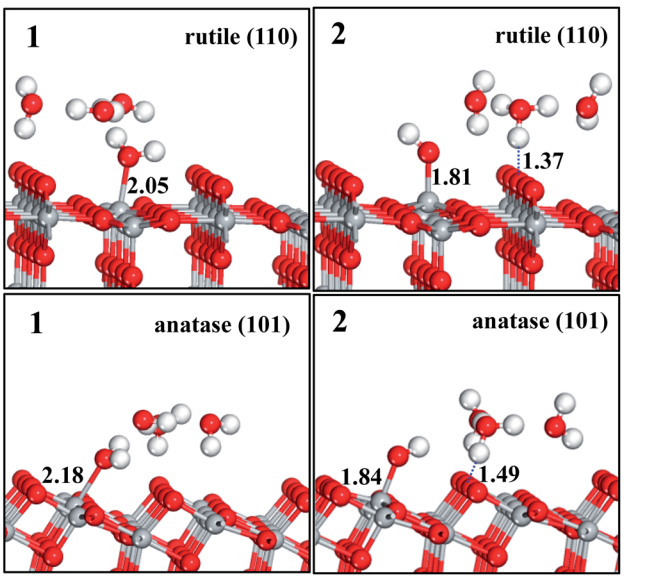

Fig. 3 Optimized structures of the adsorbed (state 1) and the dissociated (state 2) H_2O states on rutile (110) and anatase (101) surfaces in aqueous solution. Three water molecules are included as the explicit first shell solvation, and the rest of the solution is represented using the CM-MPB method. The key structural parameters (Å) are labelled. Ti, gray; O, red; H, white.

This journal is © The Royal Society of Chemistry 2014

Published on 13 February 2014. Downloaded by Fudan University on 27/03/2014 15:09:31.

which is defined by $\Delta G = G(\mathrm{X/sur}) - G(\mathrm{X}) - G(\mathrm{sur})$, where G is the free energy of the system based on DFT/CM-MPB calculations under the conditions of interest (*e.g.* vacuum, solution or charged surface). In accordance with the structural change, we found that the adsorption free energy of water without and with the surface hole are −0.86 and −1.01 eV, respectively. The results for H_2O on anatase (101) are quite similar to those on rutile (110), both in structure and in energetics, as summarized in Table 1.

In Fig. 4, we show the calculated total and projected density of states (DOS) of the adsorbed H_2O on the rutile (110) surface in the presence of the hole. We found that the VBM of rutile (110) (∼−7.5 eV) is mainly contributed from the lattice O atoms on the surface, and not from the adsorbed H_2O molecules. The major occupied O_{2p} states of the adsorbed H_2O molecule (∼−8.8 eV) are ∼1.3 eV lower compared to the VBM level of TiO_2 (also listed in Table 1). This indicates that the hole transfer from the surface (lattice O) to the adsorbed H_2O molecules is highly activated and is thus unlikely. For the weakly-bound water layer, their O atom 2p states (∼−7.8 eV) are closer but still below the VBM.

For the dissociated H_2O and the coadsorbed OH and H, we found that the OH also prefers to adsorb at the Ti_{5c} and the H will first attach to the two-coordinated bridging O (O_{2c}) on both the rutile and anatase surfaces. However, once introducing the explicit water molecules above the H (*e.g.* with three water molecules above), the formation of a solvated proton (*e.g.* $(H_2O)_2$–H_3O) is spontaneous from the energy minimization. The formation of the solvated proton occurs on both rutile and anatase, and is also independent of the surface charge conditions. The solvated proton has one H interacting with the bridging O_{2c} (see Fig. 3). This is consistent with the strong acidity of the TiO_2–H^+ species (the calculated pK_a of TiO_2–$H^+ \rightarrow TiO_2 + H^+$ is −1 for rutile[39]). Our electronic structure analysis confirms that the $(H_2O)_2$–H_3O accumulates one positive charge, indicating the formation of the solvated proton and thus the tendency of the immediate charge separation after water dissociation at the oxide/water interface. Since the state of OH* + H^+ is the only possible FS for the first proton removal reaction, we can therefore rule out the homolytic water splitting channel, route (ii), proposed above.

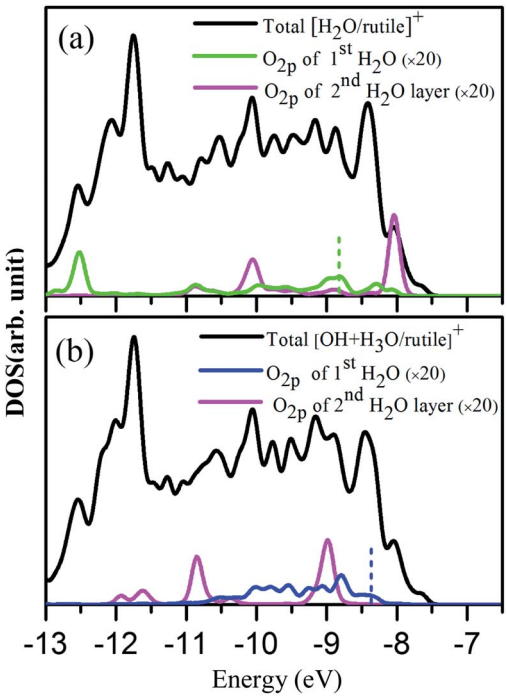

Fig. 4 The total (TDOSs, black curve) and the projected density of states (PDOSs) for (a) the adsorbed H_2O, and (b) the dissociated H_2O on the charged rutile (110) surface in aqueous solution (*via* CM-MPB). 1st H_2O: adsorbed H_2O on the surface; 2nd H_2O: H_2O molecules at the second layer. Green: O 2p states of the adsorbed H_2O; blue: O 2p states of the OH anion from the dissociated H_2O; pink: O 2p states of the H_2O molecules nearby the dissociating H_2O. The dotted lines indicate the major occupied O 2p states of the adsorbed H_2O or OH that are just below the VBM.

Table 1 The calculated free energy G of the key states in the first proton removal reaction of H_2O oxidation on rutile and anatase in aqueous solution. All free energies are with reference to the clean surface and the water in aqueous solution

State[a]	G (eV)	$d_{O\text{–}Ti}$ (Å)	$\Delta\varepsilon_{band}$[b] (eV)
Rutile (110)			
1	−0.86	2.05	−1.3
1^+	−1.01	2.04	−1.2
2	−1.03	1.81	−0.8
2^+	−1.36	1.79	−0.8
Anatase (101)			
1	−0.60	2.18	−1.3
1^+	−0.75	2.15	−1.3
2	−0.73	1.84	−0.5
2^+	−0.90	1.81	−0.5

[a] 1: adsorbed H_2O; 1^+: adsorbed H_2O on positively-charged surface; 2: adsorbed OH and H; 2^+: adsorbed OH and H on positively-charged surface. [b] $\Delta\varepsilon_{band}$: band position of the O_{2p} of the adsorbed H_2O or OH with respect to the TiO_2 VBM (see Fig. 4).

In Fig. 4b, we also compare the calculated total and projected DOS of dissociated H_2O on the rutile (110) surface in the presence of the hole, where the OH adsorbs on the surface and the H is present as a solvated proton in the water layer. The total DOS of the OH* + H^+ state is quite similar to that of the H_2O adsorbed state, except that the O_{2p} state of the adsorbed OH species is obviously more active than that of the adsorbed water molecule. The O_{2p} position of the adsorbed OH is ∼0.8 eV below the VBM of rutile, and thus ∼0.5 eV above that of the adsorbed water molecule (*cf.* Fig. 4a and b). The O_{2p} states of H_3O^+ are much lower in energy, ∼1.5 eV below the VBM in rutile, indicating that the solvated proton is already very stable and should not accept a hole from the surface.

We now summarize the calculated results for adsorbed H_2O and the OH + H^+ states on rutile and anatase in Table 1. We found that rutile generally binds more strongly for the ISs and the FSs. This can be attributed to the stronger Ti–O bond, as indicated by the shorter Ti–O bond distance on rutile. For the electronic structure, the relative band positions of the species on rutile and anatase are quite similar. It is noted that the OH

Published on 13 February 2014. Downloaded by Fudan University on 27/03/2014 15:09:31.

species has more active O_{2p} states (their band positions are closer to the VBM) compared to the adsorbed H_2O molecule. Nevertheless, neither the adsorbed OH anions nor the adsorbed H_2O are likely to act as a hole trapper. Instead, the lattice Os on the surface near the adsorbed H_2O or OH anion could be the potential hole trapper due to the enhanced electrostatic interaction between the trapped hole and the adsorbed H_2O or OH.

From the calculated energetics and band position of the adsorbed O-containing species, we can rule out the homolytic H_2O dissociation mechanism since the solvated proton is the only possible final product from the first proton removal reaction. In the following, the kinetics analysis on routes (i) and (iii) are performed to identify the most favorable pathway.

3.2 Water dissociation with and without the hole

Since route (i) and route (iii) differ mainly in the mechanism of H_2O dissociation, *i.e.* whether the hole directly participates in the O–H bond breaking of the adsorbed H_2O, we have utilized the charged-slab DFT/CM-MPB method to investigate the water dissociation kinetics in the presence and absence of the hole. In the above section, we showed that the hole transfer is thermodynamically unfavorable since the VBM of TiO_2 is far above the O_{2p} level of the adsorbed H_2O molecule (the IS). It is thus expected that the electronic structure of the TS of the O–H bond breaking should determine largely whether the presence of the hole can assist the H_2O dissociation.

On the rutile (110) and anatase (101) surfaces, we first searched for the TS of the O–H bond breaking of one H_2O molecule in vacuum conditions on the charged surface, which serves as the benchmark to compare the energetics using different DFT functionals. We found that using the PBE functional, the dissociation barrier is 0.22 eV and 0.60 eV (without ZPE correction) on rutile and anatase, respectively. The corrections to the barriers are +0.13 eV and +0.08 eV respectively for the reaction on the two surfaces, by switching the functional from PBE to the hybrid HSE06 functional. This is reasonable as the pure DFT functional tends to underestimate the reaction barrier.[40] Since the error introduced by the functional is not large, *i.e.* ~0.1 eV within the typical systematic error of DFT calculations, it indicates that the O–H bond breaking kinetics concerned here are in fact not sensitive to the DFT functional, and below we will use the PBE functional mainly in combination with the charged-slab DFT/CM-MPB method for investigating the H_2O dissociation on different surfaces.

Next, we examined the influence of the surface hole on the barrier of the H_2O dissociation in aqueous solution *via* the CM-MPB model. On the neutral surface, the H_2O dissociation free energy barrier is calculated to be 0.19 eV on rutile and 0.39 eV on anatase in aqueous solution. The barrier remains essentially the same when the surface is positively charged (with hole), *i.e.* 0.19 eV and 0.38 eV on the two surfaces. These calculated TSs on rutile are shown in Fig. 5a and b. Obviously, the presence of the surface hole does not influence much on the O–H breaking barrier. Instead, the surface structure is critical to the O–H bond breaking. Using microkinetics and assuming the same pre-exponential factor, it can be estimated that the water splitting on rutile is 3 orders of magnitude faster than on anatase at ambient conditions (300 K).

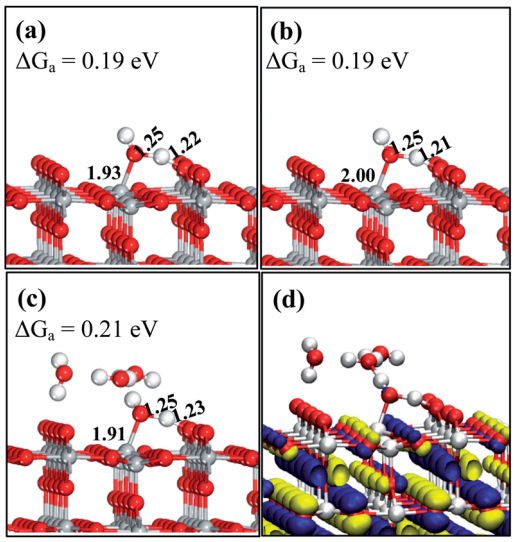

Fig. 5 The calculated TS and barrier (ΔG_a, eV) for H_2O dissociation on the rutile (110) surface under different conditions. (a) On the charged surface (with hole) in aqueous solution (CM-MPB); (b) on the neutral surface (without hole) in aqueous solution (CM-MPB). (c) On the neutral surface (without hole) in aqueous solution (with both implicit and explicit solvation). (d) 3D isosurface contour plots of the HOMO for the TS of H_2O splitting (both the hybrid HSE06 and PBE functionals provide a consistent picture). The isosurface value is set as $\pm$0.02 e Å^{-3}. The key structural parameters (Å) are labelled. Ti, gray; O, red; H, white.

To further examine the possible contribution of the short-range polarization due to the explicit solvation, we also added three explicit H_2O molecules nearby the dissociating H_2O molecule and re-searched the IS and the TS for the H_2O dissociation reaction on the neutral surfaces. The calculated TS is shown in Fig. 5c, and the barrier is found to be 0.21 eV on rutile, which is also similar to their counterparts without the explicit H_2O solvation. This indicates that the CM-MPB model can describe well the kinetics of the O–H bond breaking of adsorbed H_2O, where the oxide surface with positive Ti and negative O atoms interacts strongly with the dissociating TS complex.

It is important to ask why the presence of the surface hole does not promote the O–H bond breaking of H_2O molecules. To this end, we have analyzed the electronic structure of the O–H bond breaking TS. Shown in Fig. 5d is the 3D isosurface contour plots of the VMB (HOMO) for the TS (PBE and HSE06 functionals provide a consistent picture). On both rutile (110) and anatase (101), we found that the spatial distributions of the hole are located mainly on the surface (lattice O), not on the TS complex. This explains qualitatively why the presence of the hole does not promote the O–H bond breaking.

Quantitatively, we can also interpret the influence of the hole on the reaction barrier of O–H bond breaking according to the partial derivative, $\partial E_a/\partial n$, where n is the number of electrons in the system. $\partial E_a/\partial n$ can be expressed as a function of the eigenvalue of the HOMO (ε_{HOMO}) at the IS and the TS, as derived in eqn (7) and (8):

This journal is © The Royal Society of Chemistry 2014

Published on 13 February 2014. Downloaded by Fudan University on 27/03/2014 15:09:31.

$$\frac{\Delta E_a}{\Delta n} = \frac{E_a(N) - E_a(N-\Delta n)}{\Delta n} = \frac{E_{TS}(N) - E_{TS}(N-\Delta n)}{\Delta n} - \frac{E_{IS}(N) - E_{IS}(N-\Delta n)}{\Delta n} \quad (7)$$

$$\frac{E_a}{n} \approx \varepsilon_{HOMO}(TS) - \varepsilon_{HOMO}(IS) = \Delta\varepsilon_{HOMO} \quad (8)$$

where Δn is the change of the number of electrons in the system, and $\frac{E - E(N-\Delta n)}{\Delta n} \approx \varepsilon_{HOMO}$ is based on the DFT theorem, which states that the HOMO is the derivative of the free energy of the electrons (G) to the number of electrons (N).[41] Eqn (8) shows that the smaller the change for the HOMO level from the IS to the TS ($\Delta\varepsilon_{HOMO}$) at the charge-neutral conditions (*i.e.* $n = 0$), the smoother the slope of the barrier against the number of electrons. From our calculations, we found that $\Delta\varepsilon_{HOMO}$ for rutile and anatase is rather small, only −0.05 and 0.03 eV, respectively. This indicates that the barrier is not sensitive to the change of the number of electrons in the system, as indeed found from the calculated barriers with and without the hole.

3.3 The overall mechanism

The above results show that the H_2O dissociation is activated on TiO_2 surfaces and cannot be promoted by the surface hole. It is therefore reasonable that the capture of the hole occurs after the dissociation of H_2O. It is the final state of the H_2O dissociation, *i.e.* the OH anion and the solvated proton, state 2, that captures a hole to form the state 2^+. In the state 2^+, the hole may be transferred to the OH anion to form an OH radical or be trapped on the lattice O nearby the OH anion. According to the electronic structure shown in Fig. 4b, the latter picture could be thermodynamically more likely.

The overall mechanism of the first proton removal of water on TiO_2 can thus be described by two elementary steps: (1) heterolytic H_2O dissociation, H_2O/sur → [H···OH]/sur → OH^-/sur + H_3O^+(aq); and (2) the hole transfers to the surface O nearby the adsorbed OH anion, OH^-*/sur + hole$^+$ → [OH/sur]. Based on the charged-slab DFT/CM-MPB calculations, we have obtained the free energy profile of the reaction on rutile (110) and anatase (101), as shown in Fig. 6.

Fig. 6 shows that the first proton removal reaction occurs more favorably on the rutile surface compared to that on the anatase surface. The overall energetics can be summarized as follows. The adsorption of H_2O on rutile (110) (state 1) is exothermic by 0.86 eV, which is 0.26 eV lower than that on anatase (101) with respect to H_2O in solution. The free energy barrier of H_2O dissociation is 0.19 eV on rutile and 0.39 eV on anatase. The charge transfer occurs after the H_2O dissociation, *i.e.* 2 + hole$^+$ → 2^+, with the free energy change being −0.33 eV and −0.17 eV on rutile and anatase, respectively. Compared with anatase, the final state 2^+ on rutile is better stabilized. Overall, this photocatalytic deprotonation reaction, *i.e.* H_2O* + hole$^+$ → OH* + H^+(aq), is exothermic by 0.50 eV on rutile (110) and 0.30 eV on anatase (101). It is clear that the photocatalytic water splitting occurs preferentially on rutile, compared with anatase.

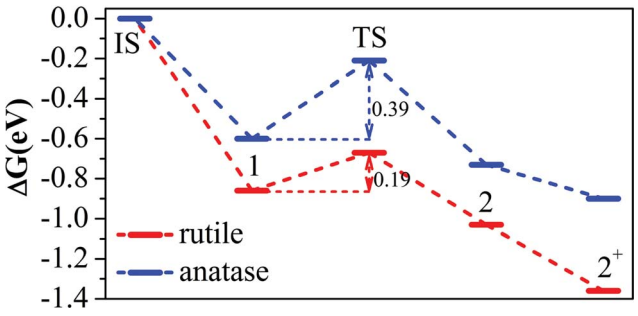

Fig. 6 Free energy profiles for the first proton removal reaction in photocatalytic H_2O splitting on rutile (110) and anatase (101) surfaces.

4. Discussion

Our results show that the key elementary step of the first proton removal for water oxidation is the O–H bond breaking, which is an activated process even at the high overpotential conditions of TiO_2 (*i.e.* with the ultraviolet radiation). Importantly, the reaction is surface structure-sensitive and the activity of rutile is much higher. The calculated results support the conventional view that the rutile phase is more active than anatase for water oxidation.

From the electronic structure, we can rule out that the position of the VBM is the cause for the enhanced photoactivity of the rutile surface compared to that of the anatase surface. By adding/subtracting the hole in the reaction, we found that the presence of the hole that is present at the VBM of the oxide surfaces at the ISs in fact does not promote the O–H bond breaking. The hole does not have a significant spatial distribution on the O–H bond breaking TS complex. This finding is important, implying that the current DFT functionals could provide good energetics for the water oxidation reaction, as also confirmed from the barriers using the PBE functional and the HSE06 functional.

It is natural to ask what causes the surface structure sensitivity for the O–H bond breaking. We first evaluated the stability of the adsorbed H on the bridging O_{2c} on rutile (110) and on anatase (101), considering that the bridging O accepts the H during the O–H bond breaking. By using the charged-slab DFT/CM-MPB calculations, we found that the adsorption free energy of H^+ on both surfaces is almost identical, *i.e.*, ∼0.15 eV. This indicates that the Lewis basicity of the oxide lattice O_{2c} are similar and should not be the cause for the activity difference between the surfaces.

Next, we compared the adsorption of H_2O and OH on the rutile (110) and anatase (101) surfaces. From Table 1, we can see that the H_2O states and the dissociated OH/H^+ states are generally more stable on rutile compared to on anatase. Overall, the dissociation of H_2O on rutile (*i.e.* 1 → 2) is only slightly more favorable (0.17 eV on rutile *vs.* 0.13 eV on anatase). Considering the much larger barrier difference (∼0.2 eV) for the O–H bonding breaking between on rutile and anatase, the thermodynamics alone cannot fully explain the activity difference.

Published on 13 February 2014. Downloaded by Fudan University on 27/03/2014 15:09:31.

By closely inspecting the calculated TS of H_2O dissociation, we can finally attribute the higher activity of rutile to the more favorable local geometrical structure, which can better stabilize the TS of the O–H bond breaking. On rutile (110), we found that the distance between the exposed Ti_{5c} and the O_{2c} is 3.53 Å, whilst it is 3.92 Å on anatase (101) (also see Fig. 1). As a result, the distance between the O (in H_2O) and the lattice O_{2c} on rutile (110) is 2.46 Å at the TS, which is 0.05 Å shorter than that on anatase (101). Consistently, the distance between the O (in H_2O) and the Ti_{5c} is 1.93 Å at the TS (Fig. 5a), which is 0.16 Å shorter than that on anatase (101). Therefore, the water molecule can dissociate with a more favorable geometry on rutile, in which the TS complex has a better contact with both the Ti_{5c} (bonding with OH) and the O_{2c} (bonding with H). We suggest that the surface structure sensitivity of water oxidation can be correlated to the geometrical separation between the exposed Ti_{5c} cation and its nearest O_{2c} anion, $d_{Ti5c–O2c}$, on the surface.

$d_{Ti5c–O2c}$, as a simple geometrical descriptor, may be utilized to rationalize the experimental debate on the activity of water oxidation on TiO_2. Using the bulk-truncated structure, we have measured $d_{Ti5c–O2c}$ for a series of common low-Miller TiO_2 surfaces, including those from rutile,[42] anatase,[43] brookite[44] and TiO_2(II) phases,[45] as shown in Table 2. Interestingly, we found that in addition to rutile (110), the rutile (101) (equivalent (011)) and (001) surfaces also exhibit a short $d_{Ti5c–O2c}$, indicating that these surfaces could be good candidates as the active site for water splitting. Indeed, Ohno *et al.*,[46] with scanning electron microscopy, observed that rutile (011) shows high activity for water oxidation ($PtCl_6^{2-}$ as the electron acceptor).

It should be pointed out that the other phases of TiO_2 may possess even higher photoactivity for water splitting based on the structural parameter, $d_{Ti5c–O2c}$. From Table 2, we found that among the surfaces/phases investigated, the TiO_2(II) phase has the shortest $d_{Ti5c–O2c}$ on its (110) and (111) surfaces. In particular, the (111) surface is known to be the most stable surface of TiO_2(II) according to experiments and also our own calculations. This finding may help to understand the experimental findings on the enhanced photoactivity on TiO_2 composites containing multiple phases. For example, Zhang *et al.*[9] have found that the photocatalytic activity of TiO_2 can be enhanced up to four times with respect to the pure phase. The composite catalyst could contain a variety of active sites with different local geometries, which could provide a more favorable local bonding environment for H_2O adsorption and splitting. Further studies along this line are needed to resolve the active site from the atomic level in TiO_2 composite catalysts.

Table 2 The distance (Å) between the Ti_{5c} cation and its nearest O_{2c} anion on the TiO_2 surfaces. The data is taken from the surfaces that can expose only the Ti_{5c} cations and O_{2c} anions

	Rutile	Anatase	Brookite	TiO_2(II)
(110)	3.53	—	3.45	3.21
(101)	3.52	3.92	—	—
(111)	4.13	—	3.45	3.21
(100)	4.13	4.34	3.67	3.50
(010)	4.13	4.33	—	—
(011)	3.52	3.92	—	—
(001)	—	4.31	3.72	3.64
(112)	—	4.32	—	—

5. Conclusions

This work represents the first theoretical attempt to resolve the kinetics of the key step of photocatalytic water oxidation, $H_2O + hole^+ \rightarrow OH + H^+$, on two important TiO_2 surfaces, rutile and anatase. To correctly compute the kinetics of the H_2O dissociation under photocatalytic conditions in the aqueous solution, the charged-slab DFT/CM-MPB method is developed and utilized to correct the band levels of the oxide and simultaneously take into account the electrical double-layer effect at the solid–liquid interface. The theoretical results have been thoroughly compared with experimental results and high-level hybrid functional HSE06 calculations. The theory shows that the photocatalytic water splitting on TiO_2 is both surface- and phase-sensitive, and the design of new catalysts towards efficient photocatalytic water splitting can be facilitated by focusing on the catalytic ability of the surface for water O–H bond breaking. Our main results are outlined as follows.

(i) The rutile (110) surface is more active for water splitting kinetically compared to anatase (101), with the calculated barrier of O–H bond breaking on rutile being ~0.2 eV lower than on anatase. The higher activity of rutile is not due to the redox level of the hole (the position of the valence band maximum), but caused by the more favorable local bonding geometry of the surface, which reduces the barrier of the O–H bond breaking.

(ii) The photogenerated hole cannot promote the O–H bond breaking, and the O–H bond splitting of water is basically a surface–catalytic reaction driven only by heat. The hole transfer occurs after the H_2O dissociation when the surface O nearby the dissociated OH anion traps the hole.

(iii) The solid–liquid interface plays an important catalytic role to stabilize and remove protons from the reaction site, which effectively avoids the charge-recombination of the dissociated OH anion with the nascent proton.

Acknowledgements

We acknowledge the National Science Foundation of China (21173051, 21361130019), the 973 program (2011CB808500, 2013CB834603), the Science and Technology Commission of Shanghai Municipality (08DZ2270500), and the Program for Professor of Special Appointment (Eastern Scholar) at Shanghai Institute of Higher Learning for financial support.

Notes and references

1 (*a*) M. A. Henderson, *Surf. Sci. Rep.*, 2011, **66**, 185; (*b*) J. Tang, J. R. Durrant and D. R. Klug, *J. Am. Chem. Soc.*, 2008, **130**, 13885; (*c*) C. Gomes Silva, R. Juárez, T. Marino, R. Molinari and H. García, *J. Am. Chem. Soc.*, 2010, **133**, 595; (*d*) M. Grätzel, *Nature*, 2001, **414**, 338; (*e*) Z. Yi, J. Ye, N. Kikugawa, T. Kako, S. Ouyang, H. Stuart-Williams,

 This journal is © The Royal Society of Chemistry 2014

Published on 13 February 2014. Downloaded by Fudan University on 27/03/2014 15:09:31.

H. Yang, J. Cao, W. Luo, Z. Li, Y. Liu and R. L. Withers, *Nat. Mater.*, 2010, **9**, 559; (*f*) K. Maeda and K. Domen, *J. Phys. Chem. Lett.*, 2010, **1**, 2655; (*g*) K. I. Hadjiivanov and D. G. Klissurski, *Chem. Soc. Rev.*, 1996, **25**, 61.

2 (*a*) G. Giorgi, M. Palummo, L. Chiodo and K. Yamashita, *Phys. Rev. B: Condens. Matter Mater. Phys.*, 2011, **84**, 073404; (*b*) R. Nakamura and Y. Nakato, *J. Am. Chem. Soc.*, 2004, **126**, 1290; (*c*) A. Imanishi, T. Okamura, N. Ohashi, R. Nakamura and Y. Nakato, *J. Am. Chem. Soc.*, 2007, **129**, 11569.

3 A. Fujishima and K. Honda, *Nature*, 1972, **238**, 37.

4 T. Ohno, D. Haga, K. Fujihara, K. Kaizaki and M. Matsumura, *J. Phys. Chem. B*, 1997, **101**, 6415.

5 K. Fujihara, T. Ohno and M. Matsumura, *J. Chem. Soc., Faraday Trans.*, 1998, **94**, 3705.

6 (*a*) T. Ohno, K. Fujihara, K. Sarukawa, F. Tanigawa and M. Z. Matsumura, *Phys. Chem.*, 1999, **213**, 165; (*b*) S. J. Tan, H. Feng, Y. F. Ji, Y. Wang, J. Zhao, A. D. Zhao, B. Wang, Y. Luo, J. L. Yang and J. G. Hou, *J. Am. Chem. Soc.*, 2012, **134**, 9978.

7 T. Ohno, K. Sarukawa, K. Tokieda and M. Matsumura, *J. Catal.*, 2001, **203**, 82.

8 R. I. Bickley, T. Gonzalez-Carreno, J. S. Lees, L. Palmisano and R. J. D. Tilley, *J. Solid State Chem.*, 1991, **92**, 178.

9 J. Zhang, Q. Xu, Z. Feng, M. Li and C. Li, *Angew. Chem., Int. Ed.*, 2008, **47**, 1766.

10 L. Kavan, M. Grätzel, S. E. Gilbert, C. Klemenz and H. J. Scheel, *J. Am. Chem. Soc.*, 1996, **118**, 6716.

11 A. Y. Ahmed, T. A. Kandiel, T. Oekermann and D. Bahnemann, *J. Phys. Chem. Lett.*, 2011, **2**, 2461.

12 S. Y. Chen and L. W. Wang, *Chem. Mater.*, 2012, **24**, 3659.

13 (*a*) A. Valdés, Z. W. Qu, G. J. Kroes, J. Rossmeisl and J. K. Nørskov, *J. Phys. Chem. C*, 2008, **112**, 9872; (*b*) A. ValdéS and G. J. Kroes, *J. Phys. Chem. C*, 2010, **114**, 1701; (*c*) U. Aschauer, Y. He, H. Cheng, S.-C. Li, U. Diebold and A. Selloni, *J. Phys. Chem. C*, 2009, **114**, 1278.

14 (*a*) Q. Guo, C. Xu, Z. Ren, W. Yang, Z. Ma, D. Dai, H. Fan, T. K. Minton and X. Yang, *J. Am. Chem. Soc.*, 2012, **134**, 13366; (*b*) A. Tilocca and A. Selloni, *J. Chem. Phys.*, 2003, **119**, 7445; (*c*) C. Sun, L.-M. Liu, A. Selloni, G. Q. Lu and S. C. Smith, *J. Mater. Chem.*, 2010, **20**, 10319.

15 (*a*) A. Fujishima, X. Zhang and D. A. Tryk, *Surf. Sci. Rep.*, 2008, **63**, 515; (*b*) R. Beranek, *Adv. Phys. Chem.*, 2011, 1.

16 J. M. Soler, E. Artacho, J. D. Gale, A. Garcia, J. Junquera, P. Ordejon and D. Sanchez-Portal, *J. Phys.: Condens. Matter*, 2002, **14**, 2745.

17 J. Junquera, Ó. Paz, D. Sánchez-Portal and E. Artacho, *Phys. Rev. B: Condens. Matter Mater. Phys.*, 2001, **64**, 235111.

18 N. Troullier and J. L. Martins, *Phys. Rev. B: Condens. Matter Mater. Phys.*, 1991, **43**, 1993.

19 J. P. Perdew, K. Burke and M. Ernzerhof, *Phys. Rev. Lett.*, 1996, **77**, 3865.

20 (*a*) H.-F. Wang and Z.-P. Liu, *J. Am. Chem. Soc.*, 2008, **130**, 10996; (*b*) C. Shang and Z.-P. Liu, *J. Chem. Theory Comput.*, 2010, **6**, 1136; (*c*) X.-J. Zhang, C. Shang and Z.-P. Liu, *J. Chem. Theory Comput.*, 2013, **9**, 5745.

21 (*a*) J. L. Fattebert and F. Gygi, *Phys. Rev. B: Condens. Matter Mater. Phys.*, 2006, **73**, 115124; (*b*) J.-L. Fattebert and F. Gygi, *Int. J. Quantum Chem.*, 2003, **93**, 139; (*c*) H.-F. Wang and Z.-P. Liu, *J. Phys. Chem. C*, 2009, **113**, 17502.

22 M. K. Y. Chan and G. Ceder, *Phys. Rev. Lett.*, 2010, **105**, 196403.

23 Y.-H. Fang and Z.-P. Liu, *J. Am. Chem. Soc.*, 2010, **132**, 18214.

24 Y.-H. Fang, G.-F. Wei and Z.-P. Liu, *Catal. Today*, 2013, **202**, 98.

25 Y.-F. Li and Z.-P. Liu, *Phys. Chem. Chem. Phys.*, 2013, **15**, 1082.

26 (*a*) Y.-H. Fang, G.-F. Wei and Z.-P. Liu, *J. Phys. Chem. C*, 2013, **117**, 7669; (*b*) D. Chen, Y. H. Fang and Z. P. Liu, *Phys. Chem. Chem. Phys.*, 2012, **14**, 16612.

27 P. Mori-Sánchez, A. J. Cohen and W. Yang, *Phys. Rev. Lett.*, 2008, **100**, 146401.

28 A. J. Cohen, P. Mori-Sánchez and W. Yang, *Phys. Rev. B: Condens. Matter Mater. Phys.*, 2008, **77**, 115123.

29 Y. F. Li and Z. P. Liu, *Phys. Chem. Chem. Phys.*, 2013, **15**, 1082.

30 S. Trasatti, *Electrochim. Acta*, 1991, **36**, 1659.

31 J. Cheng and M. Sprik, *Phys. Rev. B: Condens. Matter Mater. Phys.*, 2010, **82**, 081406.

32 J. Vandevondele, M. Krack, F. Mohamed, M. Parrinello, T. Chassaing and J. Hutter, *Comput. Phys. Commun.*, 2005, **167**, 103.

33 M. Guidon, J. R. Hutter and J. Vandevondele, *J. Chem. Theory Comput.*, 2010, **6**, 2348.

34 (*a*) M. E. Arroyo-De Dompablo, A. Morales-García and M. Taravillo, *J. Chem. Phys.*, 2011, **135**, 054503; (*b*) F. Labat, P. Baranek, C. Domain, C. Minot and C. Adamo, *J. Chem. Phys.*, 2007, **126**, 154703.

35 Y. Tamaki, A. Furube, M. Murai, K. Hara, R. Katoh and M. Tachiya, *J. Am. Chem. Soc.*, 2005, **128**, 416.

36 Y. F. Li, Z. P. Liu, L. L. Liu and W. G. Gao, *J. Am. Chem. Soc.*, 2010, **132**, 13008.

37 F. Allegretti, S. O'Brien, M. Polcik, D. I. Sayago and D. P. Woodruff, *Phys. Rev. Lett.*, 2005, **95**, 226104.

38 P. M. Kowalski, B. Meyer and D. Marx, *Phys. Rev. B: Condens. Matter Mater. Phys.*, 2009, **79**, 115410.

39 J. Cheng and M. Sprik, *J. Chem. Theory Comput.*, 2010, **6**, 880.

40 (*a*) J. P. Perdew and A. Zunger, *Phys. Rev. B: Condens. Matter Mater. Phys.*, 1981, **23**, 5048; (*b*) Y. Zhang and W. Yang, *J. Chem. Phys.*, 1998, **109**, 2604; (*c*) J.-W. Song, T. Hirosawa, T. Tsuneda and K. Hirao, *J. Chem. Phys.*, 2007, **126**, 154105; (*d*) L. Deng, V. Branchadell and T. Ziegler, *J. Am. Chem. Soc.*, 1994, **116**, 10645.

41 (*a*) W. Yang, Y. Zhang and P. W. Ayers, *Phys. Rev. Lett.*, 2000, **84**, 5172; (*b*) J. P. Perdew, R. G. Parr, M. Levy and J. L. Balduz Jr, *Phys. Rev. Lett.*, 1982, **49**, 1691.

42 D. Wang, D. Choi, Z. Yang, V. V. Viswanathan, Z. Nie, C. Wang, Y. Song, J.-G. Zhang and J. Liu, *Chem. Mater.*, 2008, **20**, 3435.

43 A. Vittadini, A. Selloni, F. P. Rotzinger and M. Grätzel, *Phys. Rev. Lett.*, 1998, **81**, 2954.

44 X.-Q. Gong and A. Selloni, *Phys. Rev. B: Condens. Matter Mater. Phys.*, 2007, **76**, 235307.

45 A. El Goresy, M. Chen, P. Gillet, L. Dubrovinsky, G. Graup and R. Ahuja, *Earth Planet. Sci. Lett.*, 2001, **192**, 485.

46 T. Ohno, K. Sarukawa and M. Matsumura, *New J. Chem.*, 2002, **26**, 1167.